Version 3 Retrievals for the Atmospheric Chemistry Experiment Fourier Transform Spectrometer (ACE-FTS)

Chris D. Boone
Department of Chemistry, University of Waterloo
Waterloo, Ontario, Canada, N2L 3G1

Kaley A. Walker
Department of Physics, University of Toronto
Toronto, Ontario, Canada, M5S 1A7

Peter F. Bernath
Department of Chemistry and Biochemistry, Old Dominion University
Norfolk, Virginia, USA, 23529-0126

Corresponding Author: Chris Boone, cboone@uwaterloo.ca

ABSTRACT

SCISAT-1, also known as the Atmospheric Chemistry Experiment (ACE), is a satellite mission for remote sensing of the Earth's atmosphere, launched on 12 August 2003. The primary instrument on the satellite is a 0.02 cm^{-1} resolution Fourier transform spectrometer (FTS) operating in the mid-infrared (750–4400 cm^{-1}). We describe the improvements implemented for the most recent processing version (3.0) of the FTS compared to the previous processing version (2.2). Problems in *a priori* pressure and temperature from October 2010 onward necessitated a further processing revision (3.5), which will be described. Changes anticipated for the next processing version (4.0) are also discussed.

1. INTRODUCTION

SCISAT-1, a small science satellite developed under the auspices of the Canadian Space Agency, features a fully tilt and shear compensated Fourier transform spectrometer (FTS) with high resolution (±25 cm maximum optical path difference) and broad spectral coverage in the mid infrared (750 to 4400 cm^{-1}). The primary goals of the SCISAT-1 Atmospheric Chemistry Experiment (ACE) mission (Bernath et al., 2005) are to (1) understand the chemical and dynamical processes that control the distribution of ozone in the stratosphere

ISBN 978-0-937194-54-9

and upper troposphere, particularly in the Arctic; (2) explore the relationship between atmospheric chemistry and climate change; (3) study the effects of biomass burning in the free troposphere; and (4) measure aerosols and clouds to reduce the uncertainties in their effects on the global energy balance.

The mission design for SCISAT-1 is based on the pioneering ATmospheric Trace Molecule Spectroscopy (ATMOS) series of missions (Gunson et al., 1996), flown four times on the NASA space shuttle. The measurement technique employed is called solar occultation, whereby the instrument measures the transmission of sunlight that has passed through the Earth's atmosphere, collecting a series of measurements as the sun rises or sets in the satellite's frame of reference. High sun spectra (solar spectra with no intervening atmosphere) are collected on each orbit and used to calculate transmittances from the atmospheric measurements, making the instruments on SCISAT-1 self-calibrating.

SCISAT-1 was launched August 12, 2003 into a circular, highly inclined orbit (650 km altitude, 74° inclination). This orbit generates up to 32 occultation events per day. For each occultation, the ACE-FTS measurements are used to generate information on atmospheric pressure and temperature, the volume mixing ratios (VMRs) for 36 different molecules and 21 subsidiary isotopologues in the most recent processing version (3.0), plus CO_2 VMR at high altitudes (above ~65 km).

The same basic strategy for atmospheric retrievals employed in ACE-FTS version 2.2 (Boone et al., 2005) is used in the version 3.0 retrievals, a global fitting approach (Carlotti, 1988) using Levenberg-Marquardt nonlinear least-squares (Press et al., 1992). This article will focus on features of the version 3.0 retrievals that are different from the previous processing version.

2. INSTRUMENTAL LINE SHAPE AND SELF-APODIZATION

The finite scan time of an FTS imposes a lower limit on the width of spectral features measured by the instrument. The instrument line shape (ILS) of an FTS is primarily governed by this finite scan time but will also include the effects of any deviations from an ideal instrument, such as off-axis rays from a finite field of view or changes in the modulation efficiency of the FTS mirrors as a function of optical path difference (Davis et al., 2001). The ILS is defined as the Fourier transform of the modulation function (MF), which can be written as follows:

$$MF(\tilde{\nu}, x) = F_{clip}(x)\eta(\tilde{\nu}, x)\frac{\sin\left(\frac{1}{2}\pi r^2\tilde{\nu}x\right)}{\frac{1}{2}\pi r^2\tilde{\nu}x},$$

where x is optical path difference in cm, $\tilde{\nu}$ is wavenumber (cm^{-1}), and r is the radius in radians of the instrument's circular field of view. The term F_{clip} is a rectangular function associated with the finite scan time of the instrument. It will be 1 for x between ± 25 cm (the maximum optical path difference for the ACE-FTS) and 0 otherwise. The third term in the above equation, with the form sinx/x, represents the effect of a finite field of view, accounting for the broadening of spectral lines that arise from off-axis rays in the instrument (Davis et al., 2001). The middle term in the above equation, η, represents any apodization applied to the measurements (other than the sinx/x term associated with off-axis rays). The finite scan time imparts a "ringing" effect to spectral features measured by the FTS, generating sidelobes when the width of a spectral feature is less than the width of the ILS (Davis et al., 2001). Apodization is a process that reduces the abruptness of the transition near ± 25 cm in F_{clip}, which decreases the amplitude of the side lobes at the expense of a broader ILS. Often, people explicitly introduce apodization functions in order to reduce the sidelobes (Norton and Beer, 1977), but there are also inherent instrumental effects that can cause the modulation function to vary with optical path difference (Hase et al., 1999). This is known as self-apodization.

The ACE-FTS suffers from major self-apodization of unknown origin. It is necessary to include an empirical function in η in the equation above in order to properly reproduce the ACE-FTS ILS. Otherwise, it is impossible to derive accurate information on the atmosphere from the ACE-FTS measurements. In version 2.2, the empirical function consisted of a series expansion in terms of optical path difference, where each of the coefficients in the expansion varied linearly with wavenumber (Boone et al., 2005). For version 3.0, a study of the ACE-FTS ILS determined that a particular shape of the empirical function for self-apodization provided a significant improvement in fitting residuals: a gradual decrease in the modulation function with increasing |x| (i.e., increase in the absolute value of optical path difference, x), combined with a sharp decrease of the modulation function for optical path difference near maximum path difference (± 25 cm). An expression was selected that reproduced this behavior with a minimum number of parameters:

$$\exp(1) * \exp\left(-\exp\left(\frac{ax^{10}}{1+bx^{10}}\right)\right)\left(1-c\frac{x}{25}\right).$$

There is nothing intrinsic about the form of the above expression; it is simply the form that gave the best residuals in the analysis of ACE-FTS spectra.

The ACE-FTS instrument has two detectors, a mercury cadmium telluride (MCT) detector that measures from 750–1810 cm^{-1}, and an Indium Antimonide (InSb) detector that measures from 1810–4400 cm^{-1}. These two detector regions were treated separately. Variation of the self-apodization effects with wavenumber was treated by using an effective field-of-view rather than true,

physical internal field-of-view for the instrument (6.25 mrad diameter). The values of the empirical parameters were determined by performing a non-linear least-squares fitting using a set of microwindows that spanned as much of the wavenumber range as possible and were restricted to high altitude (above about 40 km), where the spectral features were narrow enough that the shapes of the measured lines were close to the ILS. The fitting was performed for more than 400 occultations, and average values were then calculated.

For the MCT detector, the parameters were a = 4.403e-16, b = –9.9165e-15, c = 0.03853, and an effective field of view of 7.591 mrad diameter. For the InSb detector, the parameters were a = 2.762e-16, b = –1.009e-14, c = 0.0956, and an effective field of view of 7.865 mrad diameter. The shapes of the empirical function for the two detectors are shown in Figure 1.

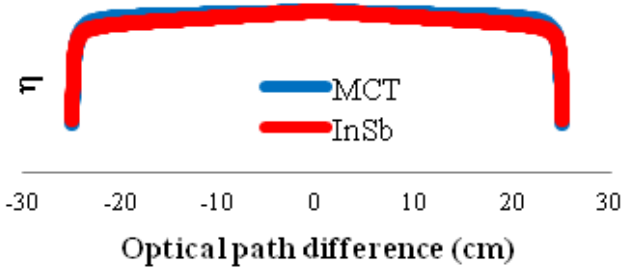

Figure 1. *Empirical functions used to account for self-apodization effects in the calculation of the ACE-FTS instrument line shape.*

3. PRESSURE/TEMPERATURE RETRIEVALS

In a validation study for the ACE-FTS version 2.2 temperatures (Sica et al., 2008), three discrepancies with other measurement sets were observed. First, a number of the retrieved temperature profiles suffered from unphysical oscillations in the mesosphere, with amplitude the order of 10 K. Second, there was a small systematic bias in retrieved temperature near 23 km. Third, there was a systematic high bias (roughly 3–6 K) in the mesosphere compared to the temperature measurements from other instruments. These problems were addressed in the development of the ACE-FTS version 3.0 pressure/temperature retrievals.

3.1. Unphysical Oscillations in Temperature Profiles

Noise on the measurement can translate into oscillations with amplitude greater than the error bars for poorly-conditioned problems such as atmospheric

inversion (Ridolfi and Sgheri, 2008). The ACE-FTS version 2.0 retrievals frequently suffered from unphysical oscillations in the retrieved VMR profiles. This problem was fixed by changing the method used to interpolate the VMRs from the measurement altitude grid onto the 1-km altitude grid employed in forward model calculations.

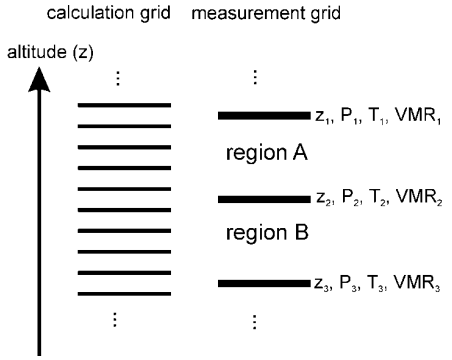

Figure 2. *A graphical representation of the two altitude grids associated with ACE-FTS retrievals. The grid on the left is the fixed 1-km grid used in forward model calculations. The grid on the right is the measurement grid, with altitudes corresponding to the measurement tangent heights. The latter grid varies from occultation to occultation, depending on orbit geometry.*

Figure 2 shows the geometry associated with the interpolation approach used in the retrieval software. With piecewise quadratic interpolation, one needs to use three measurements to generate the three coefficients:

$$X(z) = \frac{(z-z_2)(z-z_3)}{(z_1-z_2)(z_1-z_3)} X_1 + \frac{(z-z_1)(z-z_3)}{(z_2-z_1)(z_2-z_3)} X_2 + \frac{(z-z_1)(z-z_2)}{(z_3-z_1)(z_3-z_2)} X_3,$$

where X = VMR or 1/T. Looking at Figure 2, one can choose to populate the 1-km altitude grid between the upper two measurements (region A) or between the lower two measurements (region B). The latter approach was used for interpolating VMRs onto the 1-km grid in version 2.0, the processing version in which unphysical oscillations commonly appeared in the retrieved VMRs. Subsequent processing versions (2.1 and 2.2) interpolated VMRs onto the 1-km grid in region A in Figure 2, i.e., between the upper two measurements (except when VMR_3 in Figure 2 corresponds to the lowest analyzed measurement, in which case the interpolation is performed in both regions A and B). With this interpolation approach, there will be off-diagonal elements in the covariance matrix used in the least-squares analysis (between the fitting parameters VMR_1 and VMR_3) that would not be present with the alternative interpolation

approach. The correlation represented by these off-diagonal terms serves to suppress the unphysical oscillations, in a fashion similar to regularization where off-diagonal terms are artificially introduced (Ridolfi and Sgheri, 2008). Unlike explicit regularization, however, there are no decisions required regarding the "strength" of the correlation. The correlations are introduced naturally, with the only implicit constraint being the VMR profile must follow a quadratic function of altitude over the range of the three measurements employed in generating the interpolation onto the 1-km grid.

Although the interpolation approach for VMRs was changed after version 2.0, the approach for interpolating temperature onto the 1-km altitude grid remained the same, interpolating in region B as defined in Figure 2. Temperature seemed much less susceptible to unphysical oscillations, due in part to the very high signal-to-noise ratio for the CO_2 lines near 2350 cm^{-1}. However, retrieved temperature profiles in a significant number of occultations did suffer from unphysical oscillations in ACE-FTS version 2.2. Thus, the altitude interpolation approach for temperature was changed in version 3.0 processing to match what was used for the VMRs. Figure 3 shows an extreme example of unphysical oscillations in the retrieved version 2.2 temperature profile, likely exacerbated by the presence of structure (temperature inversions) in the profile. The different method for interpolating temperature onto the 1-km grid has suppressed the unphysical oscillations in the version 3.0 results.

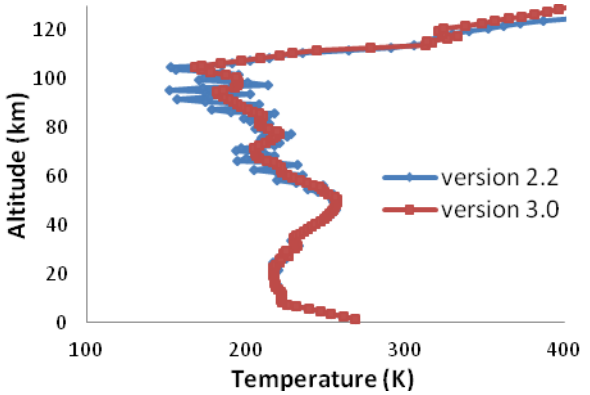

Figure 3. *Retrieved temperature profiles for ss10797. Unphysical oscillations in the version 2.2 results have been suppressed in version 3.0.*

Changes in the CO_2 microwindow set used in version 3.0 were also intended to improve the fitting stability in the mesosphere. These changes will be discussed in Section 3.5.

3.2. "Glitch" Near 23 Km

Figure 4 compares the versions 2.2 and 3.0 retrieved temperature profiles in the vicinity of the glitch identified in the temperature validation paper near 23 km (Sica et al., 2008). The anomalous behavior is evident in the version 2.2 profile. This effect arose from an empirical function used in the retrieval for pressure between 12 and 25 km, where pressure was expressed as a function of the ratio of the baseline for two points within the N_2 continuum (Boone et al., 2005). This empirical function was used to reduce the number of fitting parameters and thus improve the stability of the fitting, reducing the likelihood of getting spikes in the retrieval. However, using this empirical function appeared to yield a small inconsistency between the 12–25 km region and the 25–45 km region, leading to a discontinuity near the interface between the two altitude regions.

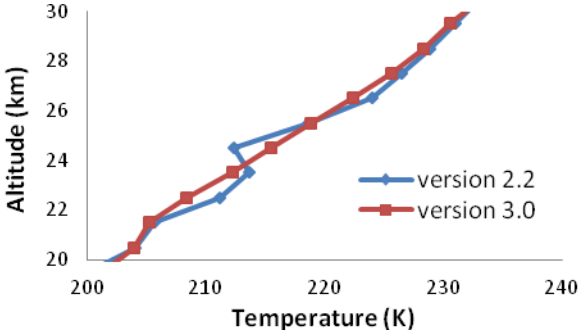

Figure 4. *Retrieved versions 2.2 and 3.0 temperature profiles in ss11614.*

For version 3.0, no empirical function is used in the retrieval. Instead, pressure at each analyzed measurement is used as a fitting parameter. Note that if there are multiple measurements within a single layer of the 1-km grid, only one of the measurements is used in the analysis, as was done in version 2.2.

Removing the empirical function for pressure necessitated changing the lower altitude limit for retrieved pressure and temperature from 12 km in version 2.2 to 15 km in version 3.0. Very few of the CO_2 microwindows used in the pressure/temperature retrievals extended below 15 km, and a few of the version 2.2 microwindows that extended below 15 km were discarded for version 3.0 because they were contaminated by solar features that did not completely cancel when atmospheric transmittances were generated from the ACE-FTS measurements. Without the constraint provided by the empirical function for pressure, the variability of the retrieval results below 15 km was too high.

A change in the way tangent heights at low altitudes were calculated in version 3.0 was adopted to improve the fitting stability at low altitudes, in part to compensate for the loss of the empirical function for pressure used in the version 2.2 fitting process. The new tangent height calculation approach will be described in more detail in Section 3.4.

3.3. Mesospheric Temperature Bias

At low altitudes in the pressure/temperature retrievals, CO_2 VMR is fixed to an assumed profile. At high altitudes, however, CO_2 VMR decreases with increasing altitude as a result of photodissociation and diffusion (Rinsland et al., 1992). In version 2.2, an empirical function was used to retrieve CO_2 VMR above about 65 km.:

$$CO_2\ VMR(z) = \frac{VMR_{strat} + a(z - z_o) + b(z - z_o)^2 + c(z - z_o)^3}{1 + d(z - z_o) + e(z - z_o)^2},$$

where VMR_{strat} is the assumed stratospheric value for CO_2 and z_o is the altitude below which CO_2 VMR is fixed in the analysis.

Without this empirical function, retrievals often gave very large spikes in retrieved CO_2 VMR accompanied by compensating spikes in retrieved temperature and pressure, clearly unphysical results. Using the empirical function provides a smoother result, relying on the assumption that there should not be much structure in CO_2 VMR at high altitudes.

A major contribution to the observed mesospheric temperature bias in version 2.2 came from the fact that no effort was made to ensure continuity between the CO_2 VMR profile fixed below ~65 km and the retrieved CO_2 VMR profile above ~65 km. Figure 5 shows an example of a retrieval result with a discontinuity between the fixed portion of the CO_2 VMR profile at lower altitudes and the retrieved portion at higher altitudes in version 2.2. This discontinuity is eliminated in version 3.0.

Version 3.0 employs the same empirical function for retrieving CO_2 VMR. However, the retrieved profile at high altitude was forced to match the fixed VMR at the interface in version 3.0. CO_2 VMR at the first measurement below the interface is also included as a fitting point in the least-squares analysis, in order to ensure the slope near the interface is at least roughly correct, generating a smooth transition between the fixed portion and the retrieved portion of the CO_2 VMR profile, as seen in Figure 5. This also appeared to help reduce the temperature bias in comparison to measurements from other instruments (Sica et al., 2008).

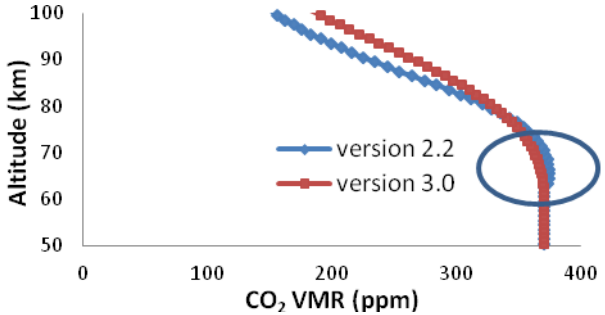

Figure 5. *CO_2 VMR profiles from versions 2.2 and 3.0 for ss11950. The portion above 65 km is retrieved, while the portion below 65 km is fixed. In version 2.2, there is a discontinuity at the interface between the fixed and retrieved portions of the profile (circled).*

Above the highest analyzed measurement in version 2.2, the empirical function for CO_2 VMR often gave a "swoop" upward (higher VMR with increasing altitude). This was unphysical behavior that was being included in the forward model calculations for pressure/temperature retrievals. For version 3.0, the portion of the CO_2 VMR profile above the highest analyzed measurement (i.e., between ~125 and 150 km) was fixed to a constant, to the value calculated from the empirical function in the tangent layer of the highest analyzed measurement.

The differences between the two profiles at higher altitudes in Figure 5 comes partly from the new ILS and partly from differences in the CO_2 microwindow set described in Section 3.5.

3.4. Calculating Tangent Height Separations

At high altitudes, accurate information on relative pointing (e.g., the change in instrument pointing from one measurement to the next) is available from simple geometry, using knowledge of the satellite's orbit to determine its position relative to the Sun at a given time. However, at low altitudes, refraction effects and phenomena that affect instrument pointing (such as clouds and aerosols) make it impossible to accurately determine even relative pointing information (much less absolute pointing) from the satellite's orbit. Pointing information provided by the SCISAT-1 satellite is unreliable. At low altitudes, we must therefore determine geometry from analysis of the ACE-FTS spectra.

In version 2.2, the equation for hydrostatic equilibrium was used to integrate separations between tangent heights downward from what was termed

the "crossover" measurement, the third measurement above 43 km (Boone et al., 2005). Tangent height separations were generated by integrating the expression for hydrostatic equilibrium:

$$\frac{dP(z)}{dz} = -g(z)\rho(z) = -\frac{g(z)m_a(z)P(z)}{kT(z)},$$

where P is pressure, T is temperature, z is altitude, g is acceleration due to gravity, ρ is density, m_a is the average molecular mass, and k is the Boltzmann constant. Note that the ideal gas law was used to write density as a function of pressure and temperature.

Version 3.0 uses the same basic strategy for determining tangent heights, integrating the hydrostatic equilibrium equation downward from the crossover measurement, using three measurements at a time and assuming a piecewise quadratic variation for 1/T. However, in version 3.0, the tangent height separations are calculated in a fashion that improves the stability of the retrieval compared to version 2.2. Looking at the measurement grid in Figure 2, when propagating the tangent height calculation downward, pressure (P_1, P_2, and P_3) and temperature (T_1, T_2, and T_3) at the measurement tangent heights are fitting parameters, known quantities for a particular iteration in the least-squares analysis. The tangent heights z_1 and z_2 are also known quantities, either fixed or calculated in a previous step of the tangent height propagation, and CO_2 VMR is fixed at low altitudes. Thus, the tangent height z_3 is the only unknown quantity and can be determined from the equation for hydrostatic equilibrium.

Because the three tangent heights are "tied together" through the assumption of piecewise quadratic variation for 1/T, there are two equivalent options to solve for z_3, integrating from z_1 to z_3 or integrating from z_2 to z_3. Integrating both sides of the equation for hydrostatic equilibrium from z_1 to z_3 yields:

$$\int_{P_1}^{P_3}\frac{dP}{P} = -\frac{g_o m_a}{k}\int_{z_1}^{z_3}\left(1-\frac{2z}{R_e}\right)\left(\frac{(z-z_2)(z-z_3)}{(z_1-z_2)(z_1-z_3)}\frac{1}{T_1} + \frac{(z-z_1)(z-z_3)}{(z_2-z_1)(z_2-z_3)}\frac{1}{T_2} + \frac{(z-z_1)(z-z_2)}{(z_3-z_1)(z_3-z_2)}\frac{1}{T_3}\right)dz,$$

where the piecewise quadratic interpolation for 1/T has been used, and the variation of the acceleration due to gravity with altitude was approximated by the expression:

$$g(z) \approx g_o\left(1-\frac{2z}{R_e}\right),$$

where R_e is the effective radius of the Earth geoid at the tangent latitude, and g_o is the acceleration due to gravity of the surface of the geoid, calculated to include the variation with latitude. Using Simpson's rule to evaluate the right hand side of the hydrostatic equilibrium integral from z_1 to z_3 yields the following expression:

$$\frac{6k}{g_o m_a}\ln\left(\frac{P_3}{P_1}\right) = \beta\left[\frac{2}{T_1}+\frac{2}{T_3}+\frac{\alpha-\beta}{\alpha}\frac{1}{T_1}-\frac{\beta^2}{\alpha(\alpha-\beta)}\frac{1}{T_2}+\frac{\alpha}{\alpha-\beta}\frac{1}{T_3}\right] - \frac{2\beta}{R_e}\left[\left(2z_1-\frac{\beta}{2}\right)\frac{1}{T_1}+\left(2z_1-\frac{3\beta}{2}\right)\frac{1}{T_3}\right] - \frac{2\beta}{R_e}\left(z_1-\frac{\beta}{2}\right)\left[\frac{\alpha-\beta}{\alpha}\frac{1}{T_1}-\frac{\beta^2}{\alpha(\alpha-\beta)}\frac{1}{T_2}+\frac{\alpha}{\alpha-\beta}\frac{1}{T_3}\right] \quad ,$$

where $\alpha = (z_1 - z_2)$ and $\beta = (z_1 - z_3)$. The variable β is the only unknown quantity in the equation and can be determined through solving a quartic equation. Similarly, the integration from z_2 to z_3 yields the following expression:

$$\frac{6k}{g_o m_a}\ln\left(\frac{P_3}{P_2}\right) = \delta\left[\frac{2}{T_2}+\frac{2}{T_3}-\frac{\delta^2}{\alpha(\alpha+\delta)}\frac{1}{T_1}+\frac{\alpha+\delta}{\alpha}\frac{1}{T_2}+\frac{\alpha}{\alpha+\delta}\frac{1}{T_3}\right] - \frac{2\delta}{R_e}\left[\left(2z_2-\frac{\delta}{2}\right)\frac{1}{T_2}+\left(2z_2-\frac{3\delta}{2}\right)\frac{1}{T_3}\right] - \frac{2\delta}{R_e}\left(z_2-\frac{\delta}{2}\right)\left[\frac{-\delta^2}{\alpha(\alpha+\delta)}\frac{1}{T_1}+\frac{\alpha+\delta}{\alpha}\frac{1}{T_2}+\frac{\alpha}{\alpha+\delta}\frac{1}{T_3}\right] \quad ,$$

where α is defined previously and $\delta = (z_2 - z_3)$. Again δ is the only unknown quantity and can be determined by solving a quartic equation.

In version 2.2, two expressions (the integral from z_1 to z_3 and the integral from z_1 to z_2) were used to generate a single cubic equation from which z_3 could be determined (Boone et al., 2005). For version 3.0, the two quartic equations are solved separately to determine two values for z_3. If the two values agree to better than 0.5 km, then the average value is used. If the difference is greater than 0.5 km, then it is a bad iteration in the least squares process. Having the two expressions from which to calculate z_3 improves the stability of the retrieval (compared to the approach used in version 2.2) and suppresses oscillatory solutions by ensuring the two integrals give a comparable result.

To further improve the fitting stability in version 3.0, a value for the tangent height of the second highest calculated measurement is included as a fitting term

with a relatively weak weighting (using an assumed error of roughly 100 m). Recall that the pressure at the crossover point is adjusted to ensure that the tangent height of highest calculated measurement falls where expected, as determined from the orbit's geometry (Boone et al., 2005). Placing a constraint on the tangent height of the second highest calculated measurement suppressed spikes that sometimes occurred during version 2.2 processing for occultations in polar spring with temperature minima at relatively high altitudes (between 30 and 40 km).

3.5. Pressure/Temperature Microwindows

Because the ILS of the ACE-FTS instrument is much broader than the spectral features being measured at high altitude, the spectral features can be strongly saturated even when the measured transmittance shows no signs of it. Figure 6 shows an example of a CO_2 line near 75 km where the monochromatic spectrum (the spectrum one would measure if the instrument had no ILS) is strongly saturated, but the minimum transmittance for the line is the order of 0.5. In this situation, the calculated spectrum starts to depend strongly on the shape of the line in the mid-wing region (rather than the shape near the center of the line), which is problematic if there are any deviations of the line shape from expectations (i.e., Voigt). The consequences of errors in spectroscopic parameters can also be magnified if the center of the line is strongly saturated.

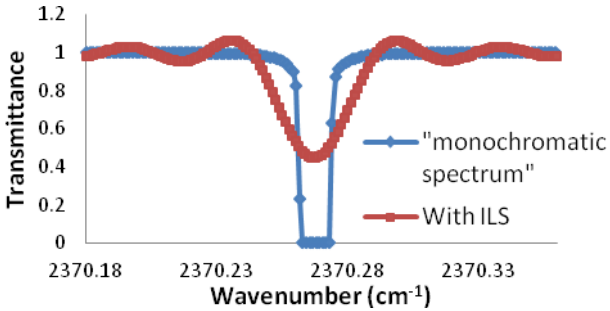

Figure 6. *The monochromatic spectrum for a CO_2 line near 75 km, along with the calculated spectrum after the monochromatic spectrum is convolved with the instrument ILS.*

In version 2.2, many of the microwindows used in the pressure/temperature retrieval extended down in altitude to where the apparent transmittance of the line was 0.1 or 0.2. Thus, at the lower altitude range of these microwindows, the

underlying spectral feature in the monochromatic spectrum was extremely saturated, much worse than the example in Figure 6, to the point where the side-lobes in the ILS were visibly attenuated.

For version 3.0, the lower altitude limits for CO_2 microwindows used in the pressure/temperature retrievals were chosen such that the center of the line was at most mildly saturated. The altitude ranges for version 3.0 microwindows were therefore much narrower than the altitude ranges for version 2.2 microwindows. Version 3.0 microwindows also reduced the number of different bands being employed in the analysis. The spectroscopic parameters for different bands of the same molecule are not always internally consistent, often measured by different laboratories on different equipment with different experimental conditions. Although one might intuitively expect that adding more information would improve retrieval results, inconsistencies between different spectral bands can often lead to biases, increased scatter, or enhanced likelihood of unphysical oscillations in the retrieved profiles.

The version 3.0 microwindow set dropped the version 2.2 microwindows from the range 3300–3380 cm^{-1} and 3570–3740 cm^{-1}. The signal-to-noise ratios in these wavenumber ranges are much worse than in the vicinity of the ν_3 CO_2 band near 2350 cm^{-1}. A number of CO_2 windows near 1960 cm^{-1} were also discarded because in some occultations they contained residual solar features that did not completely cancel when the transmittance spectra were calculated. The CO_2 microwindows used in the version 3.0 pressure/temperature retrievals are presented in the Appendix in Table A1.

3.6. Altitude Registration and CO_2 Isotopologue 3

In version 3.0, CO_2 isotopologue 3 ($^{18}O^{12}C^{16}O$) lines are used to determine the tangent heights of measurements below the analysis region (i.e., below 15 km), just as was done in version 2.2 (Boone et al., 2005). In version 2.2, the CO_2 isotopologue 3 lines were also used directly for altitude registration. In version 3.0, however, the retrieved pressure and the *a priori* pressure (from the Canadian Meteorological Center) between 15 and 25 km are used to generate the absolute altitude registration, shifting the retrieval results in altitude to achieve the best possible agreement between the two pressure profiles.

In version 2.2, intensities of the CO_2 isotopologue 3 lines were increased by 3.5%, compensating for a combination of systematic errors in the spectroscopic constants and actual differences in the VMRs between the main CO_2 isotopologue and isotopologue 3. For version 3.0, that scaling factor was adjusted to 4.3%. One extra isotopologue 3 microwindow was also added to the

analysis. The list of CO_2 isotopologue 3 lines used to generate tangent heights for measurements below 15 km is presented in Table 1.

Table 1. $^{18}O^{12}C^{16}O$ Microwindows Used to Generate Tangent Heights Below 15 km in the ACE-FTS Version 3.0 Pressure/Temperature Retrievals.

Wavenumber (cm^{-1})	Width (cm^{-1})
2610.54	0.35
2611.30	0.35
2616.45	0.40
2620.84	0.50
2626.70	0.80
2636.63	0.30

4. VOLUME MIXING RATIO RETRIEVALS

The basic procedure for retrieving VMRs in version 3.0 was the same as what was done for version 2.2 (Boone et al., 2005). Version 3.0 added a number of target species for VMR retrievals: COClF, $COCl_2$, CH_3OH, HCFC-141b, $^{13}CO_2$, $^{18}O^{12}C^{16}O$, $^{17}O^{12}C^{16}O$, $^{18}O^{13}C^{16}O$, $^{18}O^{16}O^{16}O$, $^{16}O^{18}O^{16}O$, $^{16}O^{17}O^{16}O$, $^{14}N^{15}N^{16}O$, $^{15}N^{14}N^{16}O$, $^{14}N^{14}N^{18}O$, $^{14}N^{14}N^{17}O$, $^{13}C^{16}O$, $^{12}C^{18}O$, $^{12}C^{17}O$, $^{16}O^{12}C^{34}S$, and $^{16}O^{13}C^{32}S$.

One of the big changes for version 3.0 was that different isotopologues of the same species were treated separately in the analysis, each with its own independent VMR profile. Figure 7 shows VMR profiles for two different isotopologues of ozone. Assuming a common VMR for the different isotopologues in the analysis would lead to increased residuals, which would degrade the retrieval results.

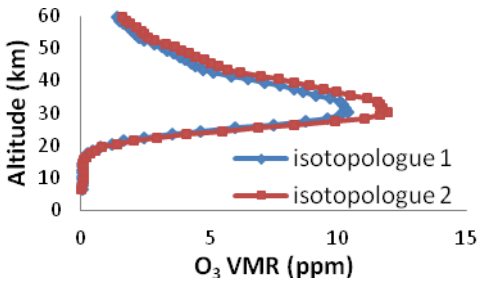

Figure 7. *Retrieved VMR profiles for O_3 isotopologue 1 ($^{16}O^{16}O^{16}O$) and isotopologue 2 ($^{18}O^{16}O^{16}O$) from ss11614.*

The altitude ranges for VMR retrievals were increased significantly in version 3.0 for many molecules. In version 2.2, very conservative altitude ranges were chosen. Version 3.0 microwindows attempted to push the retrievals to their limits, extending altitude ranges such that the lines included in the analysis were used up to where the signal was close to the noise.

For HCl and HF, atmospheric density was used to determine the upper altitude limit. These were the only two molecules for which density correlated well with the point where absorption dropped to the noise level for all geolocations and seasons.

For molecules that sometimes feature weak secondary peaks at higher altitudes (NO_2, HNO_3, H_2O_2), microwindows were chosen (wherever possible) to contain strong "interfering" lines (i.e., lines from molecules other than the target molecule) in order to ensure proper alignment between the measured and calculated spectra. The wavenumber calibration for the ACE-FTS is not reliable, and cross-correlation is used to align the measured and calculated spectra. Without a strong spectral feature to guide the cross-correlation process, spectral features near the noise limit can end up being aligned with a strong noise feature.

Where no strong interfering line was available for microwindows containing weak spectral features of the target molecule (e.g., N_2O, H_2O, O_3), the wavenumber shifts at the highest altitudes within the microwindow were constrained to match the wavenumber shifts determined at lower altitudes within that same microwindow, where the signal from the target molecule was stronger, thereby allowing an accurate determination of wavenumber shift via cross correlation.

Microwindow sets employed for ACE-FTS version 3.0 retrievals can be found at the following location: *http://www.ace.uwaterloo.ca/misc/ACE-SOC-0024-RevA-ACE-FTS_Spectroscopy__Jun212011.pdf.*

4.1. Extra Uncertainties from CO_2 Internal Consistency

The pressure/temperature retrieval at low altitudes fixes CO_2 VMR to an assumed profile. Performing a VMR retrieval for CO_2 using the same set of microwindows as was employed in the pressure/temperature retrieval, one should ideally obtain the assumed input CO_2 VMR profile. However, the limitations of the retrieval system mean that there will be some differences between the input *a priori* CO_2 VMR profile and the retrieved CO_2 profile.

In version 3.0, the discrepancies between these two profiles are used to estimate an additional "form-factor" contribution to the errors for VMR retrievals. In version 2.2, errors reported for VMR retrievals were the usual

least-squares random errors (calculated as the square root of the diagonal elements of the covariance matrix). In version 3.0, the errors are calculated as follows:

$$\frac{VMR\ error}{VMR} = \sqrt{\left(\frac{random\,VMR\ error}{VMR}\right)^2 + \left(\frac{retrieved\ CO_2 - a\ priori\ CO_2}{a\ priori\ CO_2}\right)^2},$$

under the assumption that the form factor problems that prevent internal consistency between *a priori* and retrieved CO_2 VMR will induce similar percentage errors in the retrieved VMR profiles for other molecules, independent of the random errors in the least-squares fitting.

5. LINE LIST

The line list of spectroscopic parameters employed for the ACE-FTS version 3.0 retrievals used HITRAN 2004 (Rothman et al., 2005) as a basis, but a number of updates were applied.

The line positions for HCl were taken from Coxon and Hajigeorgiou (2000). Air-broadened half-widths for H_2O were taken from Gordon et al. (2007). The parameters for H_2O_2 were taken from work by Perrin et al. (1995) and Klee et al. (1999). The parameters for C_2H_2 were taken from Lyulin et al. (2007) and Jacquemart et al. (2007). Improved line parameters for HCOOH were taken from a paper by Perrin and Vander Auwera (2007).

For OCS, correction factors were applied to the intensities of lines for the main isotopologue in HITRAN 2004 (Rothman et al., 2005). Similar correction factors should have been applied to the subsidiary isotopologues but were not, so these correction factors were used for the ACE line list.

A major update was performed on the first three isotopologues of ozone ($^{16}O^{16}O^{16}O$, $^{18}O^{16}O^{16}O$, and $^{16}O^{18}O^{16}O$) from HITRAN 2004. The line positions, intensities, and lower-state energies come from Mikhailenko et al., available at *http://smpo.iao.ru* and Plateaux et al. (1995).

Updates to the line parameters for HNO_3 were taken from Flaud et al. (2006). Additionally, the line strengths for all HNO_3 lines above 1500 cm^{-1} were decreased by 8.5%. The microwindow set for HNO_3 retrievals employs bands in different wavenumber regions that were not internally consistent. The scaling factor was applied to improve the internal consistency of retrieved HNO_3 from the two wavenumber regions employed in ACE-FTS retrievals.

Pseudolines for $COCl_2$ (Toon et al., 2001), COClF (Brown et al., 1996) and HO_2NO_2 (Brown et al., 1996) were added to the line list. There was also a set of pseudolines for C_2H_6 that filled in regions of missing spectroscopic data for the

molecule (Geoff Toon, private communication). This permitted the inclusion of C_2H_6 as an interferer in the retrievals for CH_3Cl.

A new set of H_2CO lines was obtained from A. Perrin, a preliminary set obtained in advance of the final analysis performed prior to publication (Perrin et al., 2009).

Air broadening parameters for the $X^1\Sigma^+_g$ (1-0) quadrupolar transitions of N_2 were obtained from Goldman et al. (2007). Line strengths were increased by a factor of 1.039 from their HITRAN 2004 values in order to obtain retrieved N_2 VMR profiles that matched expectations.

A strong N_2O line at 1167.29428 cm^{-1}, missing from HITRAN 2004, was added to the linelist. The positions of N_2O lines in the wavenumber range 1205–1210 cm^{-1} were adjusted to be consistent with neighboring lines.

6. VERSION 3.5

A priori information for pressure and temperature at low altitudes comes from the Canadian Meteorological Center (CMC) (Boone et al., 2005). Below 15 km, these data are taken as "truth," while between 15 and ~30 km, they serve as a first guess in the retrieval process and provide a means to perform altitude registration on the retrieval results.

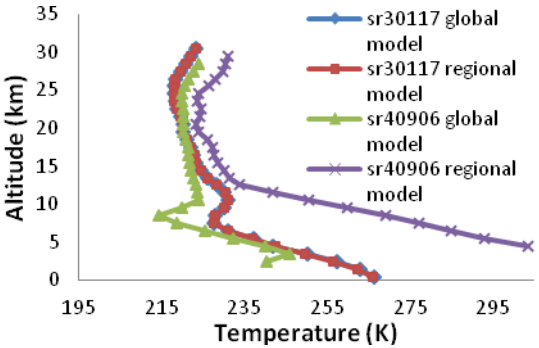

Figure 8. *A priori temperature profiles from the CMC global and regional models for sr30117 (March 2009, latitude 71.7°S) and sr40906 (March 2011, latitude 71.6 °S).*

We obtain two sets of *a priori* data from the CMC, one generated from analysis of data provided by satellites and by weather stations on the ground using a "global" model, as well as a second set of data generated using regional

models for the analysis. ACE-FTS processing always employed the results from the regional models.

From October 2010 onward, the pressure and temperature data from the regional models started to be unphysical, likely a consequence of problems with how information was extracted from the model outputs at the ACE-FTS measurement locations rather than a problem with the CMC models themselves. Figure 8 shows examples of temperature profiles from the CMC regional and global analysis data from March 2009 and March 2011. The regional and global model outputs from 2009 agree to within a fraction of a degree. The profile from the regional model in 2011 is clearly unphysical, indicating a temperature of over 300 K at altitude 5 km at a latitude of 71.4°S. The *a priori* pressure profile from the regional model also exhibits behavior uncharacteristic of the location and season for sr40906.

Bad *a priori* pressure and temperature information ruins the pressure/temperature retrievals. The results below 15 km are most strongly affected, since the *a priori* profiles were taken as truth in this region. Above 15 km, the results are less contaminated but will suffer an altitude shift due to the bad *a priori* pressure information. Note that the problems in the pressure/ temperature retrievals flow through to problems in the VMR retrievals, again with VMR results below 15 km most strongly impacted.

This issue makes the results from version 3.0 (and version 2.2, which is still being generated) from October 2010 onward unusable. Therefore, new processing versions (2.5 and 3.5) are being generated. There are no changes in the processing software from previous versions (2.2 and 3.0). The only difference will be the *a priori* information for pressure and temperature will come from the global model rather than the regional one.

7. VERSION 4.0

The next generation processing version for the ACE-FTS will feature new molecules and improvements to the retrievals for molecules in previous versions. The primary improvement will come from using a more realistic input for CO_2 VMR in the pressure/temperature retrieval. Version 3.0 employs the same shape profile regardless of location or season, and assumes a simple linear variation as a function of time, originally selected to be consistent with the HALOE experiment (Russell et al., 1993):

$$CO_2 \text{ VMR (ppm)} = 326.909 + 1.50155(t-t_o),\ t_o = 1 \text{ January } 1977,$$

where t is time in years.

A study into retrieving CO_2 VMR from ACE-FTS measurements (Foucher et al., 2009) illustrated the significant seasonal cycle for CO_2 that version 3.0 (and earlier) analysis was ignoring. A study of trends in CO_2 VMR at high altitude (where CO_2 is retrieved from the ACE-FTS rather than fixed) indicated that the assumed trend in CO_2 VMR (1.50155 ppm/year) is lower than the current accepted rate of change for CO_2 (Emmert et al., 2012).

For version 4.0, pressure/temperature retrievals will use CO_2 VMR profiles that will include variations with season and with latitude and will have an assumed rate of change that agrees better with currently expectations (a rate of change of half a percent per year will be assumed for version 4.0). Figure 9 shows some comparisons of CO_2 VMR profiles used as inputs in version 3.0 processing versus the profiles that will go into version 4.0. The shape of the CO_2 VMR profile employed for version 3.0 processing most closely resembles the shape for tropical occultations in version 4.0. In polar occultations, the shape of the CO_2 profile will be much different in version 4.0. In version 3.0, a constant VMR was assumed through the stratosphere, but in version 4.0, there will be a decline with increasing altitude, calculated based on age of air considerations. These changes in *a priori* CO_2 VMR will flow through to changes in the retrieved VMR profiles for other molecules.

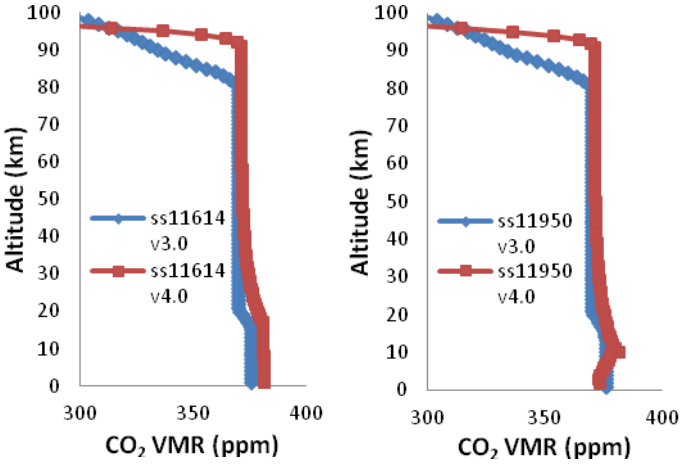

Figure 9. *A priori CO_2 VMR profiles for version 3.0 and 4.0. On the left are the profiles for ss11614, a tropical occultation. On the right are the profiles for ss11950, a polar occultation.*

Version 4.0 pressure/temperature retrievals will also allow interferences for the first time. Previously, all CO_2 microwindows employed in pressure/temperature retrievals were required to have negligible interferences from other molecules (or other isotopologues of CO_2). The lower altitude limit of 15 km in the pressure/temperature analysis arises from the fact that it is impossible to find many "clean" CO_2 microwindows below that altitude, i.e., microwindows free from significant interferences. By allowing for interferences, the pressure/temperature retrievals can be pushed lower, possibly down to 5 km, the lower limit of ACE-FTS measurements. Allowing interferers also provides more potential microwindows at high altitude, eliminating the need for the empirical function used previously to retrieve CO_2 VMR above ~65 km.

ACKNOWLEDGEMENTS

Thanks to Marty McHugh for providing the HALOE CO_2 equation and to Manuel Lopez-Puertas for providing a comparison CO_2 profile. Thanks to Geoff Toon for providing the subroutine for calculating *a priori* CO_2 VMR profiles. Funding was provided by the Canadian Space Agency and the Natural Sciences and Engineering Research Council (NSERC) of Canada, as well as the NSERC-Bomem-CSA-MSC Industrial Research Chair in Fourier Transform Spectroscopy.

REFERENCES

Bernath, P.F., et al. (2005): Atmospheric Chemistry Experiment (ACE): mission overview. *Geophys Res Lett*, vol. 32, L15S01, doi:10.1029/2005GL022386.

Boone, C.D., Nassar, R., Walker, K.A., Rochon, Y., McLeod, S.D., Rinsland, C.P., and P.F. Bernath (2005): Retrievals for the atmospheric chemistry experiment Fourier-transform spectrometer. *Appl Opt*, vol. 44 (33), pp. 7218-7231.

Brown, L.R., Gunson, M.R., Toth, R.A., Irion, F.W., Rinsland, C.P., and Goldman A. (1996): 1995 Atmospheric Trace Molecule Spectroscopy (ATMOS) linelist. *Appl Opt*, vol. 35, pp. 2828-2848.

Carlotti, M. (1988): Global-fit approach to the analysis of limb-scanning atmospheric measurements. *Appl Opt*, vol 27, pp. 3250-3254.

Chu, W.P., McCormick, M.P., Lenoble, J., Brogniez, C., and Pruvost, P. (1989): SAGE II Inversion Algorithm. *J Geophys Res, vol. 96*, pp. 8339-8352.

Coxon, J.A., and Hajigeorgiou P.G. (2000): The Radial Hamiltonians for the $X^1\Sigma^+$ and $B^1\Sigma^+$ States of HCl. *J Mol Spectrosc*, vol. 203, pp. 49-64.

Davis, S.P., Abrams, M.C. and Brault, J.W. (2001): *Fourier Transform Spectroscopy*, Academic Press, San Diego, California, USA.

Emmert, J.T., Stevens, M.H., Bernath, P.F., Drob, D.P., and C.D. Boone (2012): Observations of increasing carbon dioxide concentration in Earth's thermosphere. *Nature Geoscience*, vol. 5, pp. 868-871.

Flaud, J.-M., Brizzi, G., Carlotti, M., Perrin, A., and Ridolfi, M. (2006): MIPAS database: Validation of HNO_3 line parameters using MIPAS satellite measurements. *Atmos Chem Phys*, vol. 6, pp. 5037-5048.

Foucher, P.Y., Chédin, A., Dufour, G., Capelle, V., Boone, C.D., and Bernath, P.F. (2009): Technical Note: Feasibility of CO_2 profile retrieval from limb viewing solar occultation made by the ACE-FTS instrument. *Atmos Chem Phys*, vol. 9, pp. 2873-2890.

Gilbert, K.L., Turnbull, D.N., Walker, K.A., Boone, C.D., McLeod, S.D., Butler, M., Skelton, R., Bernath, P.F., Châteauneuf, F., and Soucy, M.-A. (2007): The onboard imagers for the Canadian ACE SCISAT-1 mission. *J Geophys Res*, vol. 112, D12207, doi:10.1029/2006JD007714.

Goldman, A., Tipping, R.H., Ma, Q., Boone, C.D., Bernath, P.F., Demoulin, P., Hase, F., Schneider, M., Hannigan, J.W., Coffey, M.T., and Rinsland, C.P. (2007): On the Line Parameters for the $X^1\Sigma^+{}_g$ (1-0) quadrupolar transitions of $^{14}N_2$. *J Quant Spectrosc Rad Transfer*, vol. 103, pp. 168-174.

Gordon, I.E., Rothman, L.S., Gamache, R.R., Jacquemart, D., Boone, C.D., Bernath, P.F., Shephard, M.W., Dalamere, J.S., and Clough, S.A. (2007): Current updates of the water vapor line list in HITRAN: A New "Diet" for air-broadened half-widths. *J Quant Spectrosc Rad Transfer*, vol. 108, pp. 389-402.

Gunson, M.R., et al. (1996): The Atmospheric Trace Molecule Spectroscopy (ATMOS) Experiment: Deployment on the ATLAS Space Shuttle missions. *Geophys Res Lett*, vol. 23, pp. 2333-2336.

Hase, F., Blumenstock, T., and Paton-Walsh, C. (1999): Analysis of the instrumental line shape of high-resolution Fourier transform IR spectrometers with gas cell measurements and new retrieval software. *Appl Opt*, vol. 38(15), pp. 3417-3422.

Jacquemart, D., Lacome, N., Mandin, J.-Y., Dana, V., Lyulin, O.M., and Perevalov, V.I. (2007): Multispectrum fitting of line parameters for $^{12}C_2H_2$ in the 3.8-μm spectral region. *J Quant Spectrosc Rad Transfer*, vol. 103, pp. 478-495.

Klee, S., Winnewisser, M., Perrin, A., and Flaud, J.-M. (1999): Absolute Line Intensities for the ν_6 Band of H_2O_2. *J Mol Spectrosc*, vol. 195, pp. 154-161.

Kuntz, M. (1997): A new implementation of the Humlicek algorithm for the calculation of the Voigt profile function. *J Quant Spectrosc Rad Transfer*, vol. 57, pp. 819-824; W. Ruyten (2004): Comment on "A new implementation of the Humlicek algorithm for the calculation of the Voigt profile function" by M. Kuntz [JQSRT 57(6) (1997) 819–824]. *J Quant Spectrosc Rad Transfer*, vol. 86, pp. 231-233.

Lyulin, O.M., Perevalov, V.I., Mandin, J.-Y., Dana, V., Gueye, F., Thomas, X., Von der Heyden, P., Decatoire, D., Regalia-Jarlot, L., Jacquemart, D., and Lacome, N. (2007): Line intensities of acetylene: Measurements in the 2.5-μm spectral region and global modeling in the Δp=4 and 6 series. *J Quant Spectrosc Rad Transfer*, vol. 103, pp. 496-523.

McElroy, C.T., Nowlan, C.R., Drummond, J.R., Bernath, P.F., Barton, D.V., Dufour, D.G., Midwinter, C., Hall, R.B., Ogyu, A., Ullberg, A., Wardle, D.I., Kar, J., Zou, J., Nichitiu, F., Boone, C.D., Walker, K.A., and Rowlands, N. (2007): The ACE-MAESTRO Instrument on SCISAT: description, performance and preliminary results. *Appl Opt*, vol. 46 (20), pp. 4341-4356.

Norton, R.H., and Beer, R. (1977): New apodizing functions for Fourier spectrometry. *J Opt Soc Am*, vol. 66, pp. 259-264; erratum, vol. 67, p. 419.

Perrin, A., Valentin, A., Flaud, J.-M., Camy-Peyret, C., Schriver, L., Schriver, A., and Arcas, P. (1995): The 7.9-μm Band of Hydrogen Peroxide: Line Positions and Intensities. *J Mol Spectrosc*, vol. 171, pp. 358-373.

Perrin, A. and Vander Auwera, J. (2007): An improved database for the 9 μm region of the formic acid spectrum. *J Quant Spectrosc Rad Transfer*, vol. 108, pp. 363-370.

Perrin, A., Jacquemart, D, Kwabia Tchana, F., and Lacome, N. (2009): Absolute line intensities measurements and calculations for the 5.7 and 3.6 μm bands of formaldehyde. *J Quant Spectrosc Rad Transfer*, vol. 110, pp. 700-716.

Plateaux, J.J., Barbe, A., and Delahaigue, A. (1995): Reims high resolution Fourier transform spectrometer -- data reduction for ozone. *Spectrochim Acta Part A*, vol. 51**,** pp. 1153-1169.

Press, W.H., Flannery, B.P., Teukolsky, S.A., and Vetterling, W.T. (1992): *Numerical Recipes in Fortran, 2nd Edition*, Cambridge University Press, New York, New York, USA.

Ridolfi, M., and Sgheri, L. (2008): A self-adapting regularization method. *Atmos Chem Phys*, vol. 8, pp. 18007-18037.

Rinsland, C.P., Gunson, M.R., Zander, R., and López-Puertas, M. (1992): Middle and upper atmosphere pressure-temperature profiles and the abundances of CO_2 and CO in the upper atmosphere from ATMOS/Spacelab 3 Observations. *J Geophys Res*, vol. 97, pp. 479-495.

Rothman, L.S., et al. (2005): The HITRAN 2004 molecular spectroscopic database. *J Quant Spectrosc Rad Transfer*, vol. 96, pp. 139-204.

Russell III, J.M., Gordley, L.L., Park, J.H., Drayson, S.R., Hesketh, D.H., Cicerone, R.J., Tuck, A.F., Frederick, J.E., Harries, J.E., and Crutzen, P.J. (1993): The Halogen Occultation Experiment. *J Geophys Res*, vol. 98, pp. 10777-10797.

Sica R.J., et al. (2008): Validation of the Atmospheric Chemistry Experiment (ACE) version 2.2 temperature using ground based and space-borne measurements. *Atmos Chem Phys*, vol. 8, pp. 35-62.

Toon, G.C., Blavier, J.-F., Sen, B., and Drouin, B.J. (2001): Atmospheric $COCl_2$ measured by solar occultation spectroscopy. *Geophys Res Lett*, vol. 28, pp. 2835-2838, doi: 10.1029/2000GL012156.

APPENDIX: PRESSURE/TEMPERATURE RETRIEVAL MICROWINDOWS

Table A1. CO_2 Microwindows Employed in the Pressure/Temperature Retrievals in ACE-FTS Version 3.0.

Center Frequency (cm^{-1})	Microwindow width (cm^{-1})	Lower altitude Limit (km)	Upper altitude Limit (km)
927.00	0.35	30	45
929.00	0.35	30	45
931.00	0.35	30	45
932.96	0.30	25	45
934.82	0.45	15	45
936.80	0.35	15	45
940.52	0.80	15	45
942.40	0.35	15	45
946.00	0.35	20	45
947.70	0.40	20	45
1899.17	0.30	30	58
1902.05	0.30	30	60
1905.16	0.40	35	45
1905.26	0.22	25	35
1906.48	0.30	30	65
1911.02	0.35	35	68
1911.12	0.30	30	35
1912.52	0.35	45	68
1914.12	0.30	30	70
1915.48	0.30	30	70

Center Frequency (cm^{-1})	Microwindow width (cm^{-1})	Lower altitude Limit (km)	Upper altitude Limit (km)
1917.06	0.35	30	70
1920.11	0.35	30	70
1924.71	0.35	40	65
1929.45	0.30	25	45
1930.90	0.27	15	45
1933.98	0.24	25	60
1934.78	0.24	22	45
1935.24	0.28	15	50
1936.44	0.30	25	50
1941.03	0.35	15	45
1950.68	0.30	15	45
1962.08	0.30	35	45
1968.64	0.30	35	45
1970.12	0.30	20	45
1975.10	0.30	15	40
2044.50	0.30	50	70
2045.97	0.30	53	73
2047.53	0.40	55	73
2049.05	0.40	53	75
2050.55	0.40	55	78
2052.10	0.30	50	79
2053.66	0.30	55	80
2055.11	0.35	60	80
2056.72	0.30	55	85
2058.24	0.40	55	85
2061.33	0.35	60	85
2062.87	0.35	60	85
2066.03	0.35	60	85
2067.52	0.35	60	83
2070.65	0.40	62	80
2072.23	0.30	57	80
2289.20	0.35	105	125
2291.50	0.30	110	125
2293.90	0.35	78	125
2296.06	0.30	110	125
2298.24	0.30	105	125
2300.40	0.30	90	125
2306.85	0.30	95	125
2313.10	0.35	95	125
2319.14	0.26	90	125
2332.37	0.30	95	125

Center Frequency (cm^{-1})	Microwindow width (cm^{-1})	Lower altitude Limit (km)	Upper altitude Limit (km)
2354.37	0.26	90	125
2361.45	0.30	90	125
2364.10	0.30	90	125
2366.63	0.30	90	125
2367.88	0.30	90	125
2369.10	0.30	90	125
2370.27	0.35	90	125
2371.43	0.30	90	125
2372.56	0.30	90	125
2373.67	0.35	90	125
2374.23	0.28	50	65
2374.75	0.40	90	125
2375.40	0.28	50	60
2375.80	0.35	90	125
2376.84	0.35	90	125
2377.85	0.35	90	125
2378.83	0.35	75	125
2379.78	0.35	90	125
2380.72	0.35	85	125
2381.62	0.35	85	125
2382.48	0.40	82	125
2383.36	0.35	82	125
2384.20	0.35	90	125
2385.02	0.40	75	125
2385.79	0.35	73	125
2386.51	0.35	70	125
2387.26	0.35	65	125
2387.96	0.35	60	80
2388.64	0.35	55	77